Article

Versatile optical frequency division with Kerr-induced synchronization at tunable microcomb synthetic dispersive waves

Grégory Moille [1,2] ✉, Pradyoth Shandilya[3], Alioune Niang[3], Curtis Menyuk [3], Gary Carter[3] & Kartik Srinivasan [1,2] ✉

Kerr-induced synchronization (KIS) provides a key tool for the control and stabilization of a dissipative Kerr soliton (DKS) frequency comb, enabled by the capture of a comb tooth by an injected reference laser. Efficient KIS relies on large locking bandwidth, meaning both the comb tooth and intracavity reference power need to be sufficiently large. Although KIS can theoretically occur at any comb tooth, large modal separations from the main pump to achieve large optical frequency division factors are often difficult or unfeasible due to cavity dispersion. While tailoring the dispersion to generate dispersive waves can support on-resonance KIS far from the main pump, this approach restricts synchronization to specific wavelengths. Here we demonstrate an alternative KIS method that allows efficient synchronization at arbitrary modes by multi-pumping a microresonator. This creates a multicolour DKS with a main and an auxiliary comb, the latter enabling the creation of a synthetic dispersive wave. As cross-phase modulation leads to a unique group velocity for both the soliton comb and the auxiliary comb, repetition rate disciplining of the auxiliary comb through KIS automatically controls the DKS microcomb. We explore this colour-KIS phenomenon theoretically and experimentally, showing control and tuning of the soliton microcomb repetition rate, resulting in optical frequency division independent of the main pump noise properties.

Optical frequency combs are, in their low-noise state, an essential component in the metrology toolbox for frequency and time measurement[1,2]. They can be used as a phase-coherent frequency multiplier/divider between the microwave and optical domains for optical frequency synthesis[3], optical clockworks[4,5], time transfer[6,7] and ultralow noise microwave generation[8,9], while also increasingly finding application in more widespread consumer technologies such as distance ranging[10]. Integrating such optical frequency combs on-chip has been a recurrent quest over the past decade, in particular with the demonstration of dissipative Kerr soliton (DKS) microcombs,

which convert a continuous-wave pump into a periodically extracted pulse train[11]. DKSs at their core rely on the dispersion compensation by Kerr nonlinearity present in several complementary metal–oxide–semiconductor-compatible materials, such as silicon nitride (Si_3N_4), allowing for low-cost and mass-scale fabrication of high-quality-factor microring[12] or Fabry–Pérot[13] resonators through which DKSs can be generated with low pump power[14]. Although the combs' technical requirements may vary from one application to another, the control and/or stabilization of their repetition rate is in general a key element[2]. In particular, optical frequency division (OFD) relies on pinning two

[1]Joint Quantum Institute, NIST/University of Maryland, College Park, MD, USA. [2]Microsystems and Nanotechnology Division, National Institute of Standards and Technology, Gaithersburg, MD, USA. [3]University of Maryland, Baltimore County, Baltimore, MD, USA. ✉e-mail: gregory.moille@nist.gov; kartik.srinivasan@nist.gov
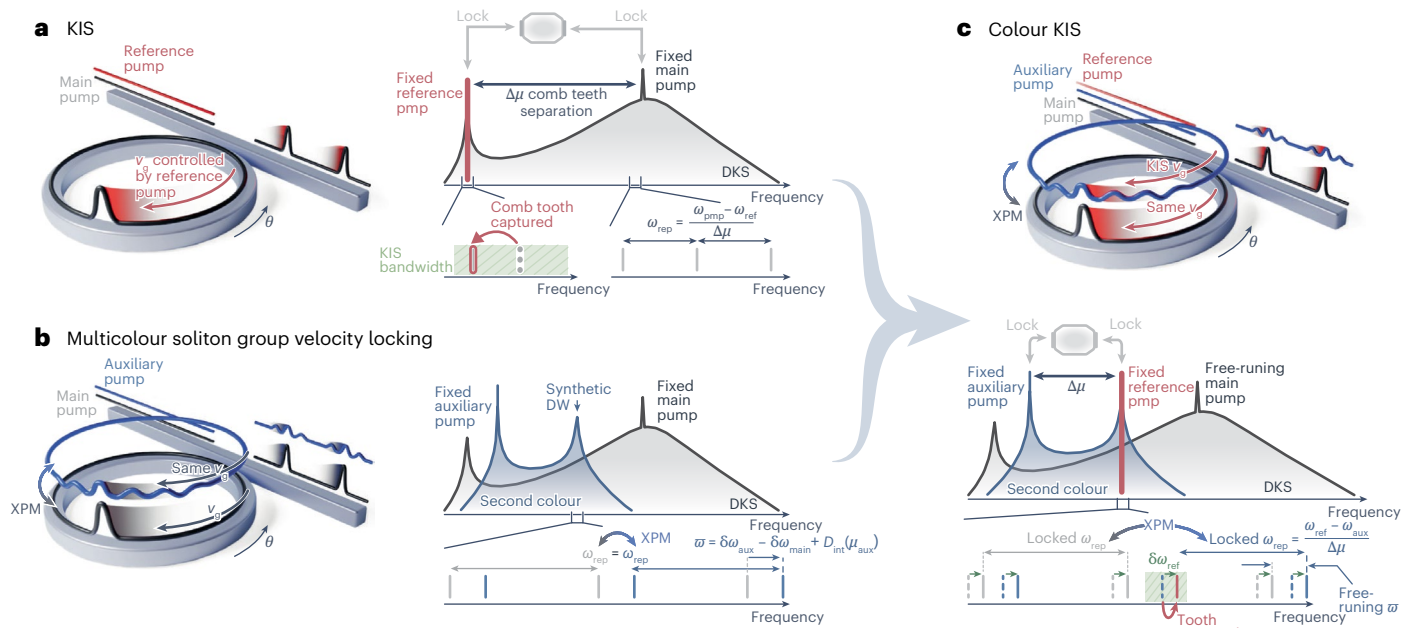
Fig. 1 | Concept of colour KIS. a, The KIS concept for OFD. A DKS is generated by driving a microring resonator with the main pump propagating in the clockwise direction of the azimuthal dimension of the microresonator (that is, along $-\theta$). An injected reference laser captures the nearest comb tooth. Any variation of frequency of the two locked pumps will be divided onto the repetition rate of the DKS by a factor $\Delta\mu$, the comb tooth separation between the two pumps, and hence the DKS group velocity (v_g) is controlled through the reference pump. **b**, Outside of synchronization, the reference pump does not capture a comb tooth. However, XPM binds the intracavity colour triggered by this auxiliary pump, making it travel at the same group velocity as the DKS. This results in a two-component comb sharing the exact same repetition rate, yet offset in CEO from one another by $\varpi = \delta\omega_{aux} - \delta\omega_{main} + D_{int}(\mu_{aux})$, accounting for the main and auxiliary pump detunings and the integrated dispersion at the auxiliary pumped mode. In this case, the repetition rate is not disciplined through OFD. However, a new phase-matching condition occurs, where a synthetic DW is created. **c**, In colour KIS, we harness both effects. The secondary colour's creation of a DW enables both large comb tooth power and an on-resonance reference pump for efficient KIS—this time at the secondary colour. However, as XPM binds the two colours together, any tuning of the repetition rate through the frequency tuning of the reference $\delta\omega_{ref}$ that is imprinted onto the secondary colour is automatically replicated onto the DKS. Hence, the auxiliary and reference pump can be independently optically locked for OFD, while the main DKS pump remains free running, as the relative comb colour offset ϖ absorbs any frequency noise from the main pump.

comb teeth to stable lasers, leveraging the fundamental property that their noise will be divided onto the repetition rate by their comb tooth separation[15]. Although on-chip operation for the laser stabilization[16] and the comb generation[17,18] can be achieved, the overall architecture mostly relies on lab-scale equipment for the comb-laser locking with only one degree of freedom (that is, the main pump). Recently, Kerr-induced synchronization (KIS) has been demonstrated as an all-optical approach to address the technical challenge of optically locking the comb[19]. In KIS, the injection of another reference pump laser into the comb-generating resonator results in the closest comb tooth snapping onto the reference (Fig. 1a), enabling external control of two comb teeth through both pumps. This method has been successfully shown to enable all-optical OFD through locking of both pumps[19,20], with performance on par with other techniques[17,21].

Although KIS greatly simplifies an optical clockwork[19,22], it can be challenging to implement for other OFD applications. First, it fixes the main pump, rendering the system stiff if low phase noise is to be achieved, and greatly limiting the choice of frequency for the reference laser that provides the second pinning point for the comb. Second, self-injection locking (SIL), which has enabled turn-key DKS generation[23–25], will in most cases be possible only at the main pump, and not at the reference pump, as the cavity dispersion creates a frequency shift between the comb line and its nearest resonance[26]. This frequency offset, when larger than the KIS bandwidth, means that resonant feedback for SIL will not be available at a frequency for which KIS can occur, thereby limiting the ability to realize a system that exploits dual SIL for turn-key DKS generation and OFD. Third, this KIS phase-locking efficiency relies on the KIS coupling energy, which can be expressed as the geometrical mean of the intracavity power of the comb tooth and the reference pump upon synchronization[19,20]. The injection of the reference laser at a dispersive wave (DW) enhances the KIS energy since the comb tooth is resonant, maximizing both the tooth and reference intracavity power. However, DWs are not always present, especially in microcombs with directly detectable, low repetition rates that are often achieved in resonators with pure quadratic dispersion. It has been shown that DW operation is not a prerequisite for KIS[20]. However it is generally advantageous for the dual pinning to occur between widely separated comb teeth, to provide a large OFD factor. Here, the sech[2] microcomb envelope greatly reduces the available comb tooth power far from the main pump, while the larger spectral offset between comb tooth and resonance (in absence of a DW) leads to poor injection of the reference into the resonator. These effects may lead to a KIS bandwidth narrower than the laser linewidth, making synchronization practically unachievable. Here we propose a scheme that uncouples the main pump soliton—which can remain free running—with the all-optical OFD enabled through KIS, by using a multicolour cavity soliton in a microring resonator[26].

Physical concept of the colour KIS

We start by reviewing multi-pumped DKS operation outside of synchronization. In this case, the second injected laser does not become a DKS comb tooth (Fig. 1b). Instead, it stimulates the formation of an auxiliary comb[26,27], with cross-phase modulation (XPM) locking the auxiliary comb and DKS comb group velocities in the cavity[28]. These two travelling wavepackets differ by only their phase velocity, so that their extraction into the access waveguide results in two frequency comb components with the same comb tooth spacing yet with a shift of carrier-envelope offset (CEO) from one another. We

refer to each component (that is, the auxiliary comb and the primary DKS) as colours, defined by their respective phase velocity (CEO in the spectral domain). Interestingly, using this scheme enables a new phase-matching condition at the second colour[29], whose location is highly flexible as it can be widely tuned by hopping between cavity modes, or finely tuned through tuning within a cavity mode, without disrupting the DKS state. This results in the creation of DW(s) that can be harnessed, for instance, for spectral extension[26,27], where high-power comb teeth can be generated at frequencies of interest. As these new DWs are not solely governed by cavity dispersion, but are instead tunable based on the secondary laser frequency (that is, tuning the CEO difference between the colours), we refer to them as synthetic DWs. Here we harness both KIS and the synthetic DWs produced in these multicolour solitons (Fig. 1c). By injecting an auxiliary laser on-resonance with a cavity mode, hence shifted from its nearest comb tooth because of the resonator dispersion, we create a second colour at the same group velocity as the DKS, but with a spectral shift of tens of gigahertz from the DKS CEO frequency. We show that the second colour, which automatically presents at least one DW, can undergo a power-efficient KIS by a reference pump (a third laser injected into the resonator). Through XPM, the KIS of the second colour is automatically transferred onto the DKS, enabling control and/or stabilization of the DKS repetition rate. Importantly, in this scheme, the main pump does not require any locking, as all its noise will be absorbed by the spectral offset between the two comb components while the repetition rate remains locked through the OFD between the auxiliary and reference lasers. Also, as this colour KIS does not impose specific requirements on the resonator dispersion, it widely expands the range of devices and scenarios in which KIS can be utilized to synchronize DKS microcombs to optical references.

Theoretical study of the colour KIS

The addition of other driving fields can be introduced in a single Lugiato–Lefever equation (LLE) accounting for their phase and azimuthal offsets[30]. Although this multipump LLE approach captures the KIS phenomenon[19], it can be challenging to study the different colours individually as they are all included in the single cavity field. Instead, one can obtain a system of nonlinearly coupled LLEs accounting for the DKS field a_{dks} and phase-offset second colour a_{sec}, both driven by their respective pump P_{main} and P_{aux}. Such formalism enables the re-normalization of their respective phase and allows study of each colour independently (see Methods for the derivation):

$$\frac{\partial a_{dks}}{\partial t} = \left(-\frac{\kappa}{2} + i\delta\omega_{main}\right)a_{dks} + i\Sigma_\mu D_{int}(\mu)A_{dks}e^{i\mu\theta}$$
$$-i\gamma L(|a_{dks}|^2 + 2|a_{sec}|^2)a_{dks} \qquad (1)$$
$$+i\sqrt{\kappa_{ext}P_{main}}$$

$$\frac{\partial a_{sec}}{\partial t} = \left(-\frac{\kappa}{2} + i\delta\omega_{aux} - iD_{int}(\mu_{aux})\right)a_{sec}$$
$$+i\Sigma_\mu D_{int}(\mu)A_{sec}e^{i\mu\theta}$$
$$-i\gamma L(2|a_{dks}|^2 + |a_{sec}|^2)a_{sec} \qquad (2)$$
$$+i\sqrt{\kappa_{ext}P_{aux}}e^{i\mu_{aux}\theta}$$

with A_{dks} and A_{sec} the respective Fourier transforms of a_{dks} and a_{sec} in the azimuthal angle θ/mode μ of the microring. The resonator properties that we are using, which include the total and external loss rate κ and κ_{ext}, the nonlinear coefficient γ and the resonator length L, can be found in Methods. The external parameters we experimentally control are the main and auxiliary pump power $P_{main} = 200$ mW and $P_{aux} = 5$ mW, respectively, μ_{aux} is the auxiliary pumped mode, and $\delta\omega_{main}$ and $\delta\omega_{aux}$ are the detuning of the main and secondary pump relative to their respective pumped modes $\mu = 0$ and $\mu = \mu_{aux}$. As the two colours are coupled

through XPM, they show the same group velocity but phase slip relative to one another, resulting in two equally spaced comb components offset from one another by $\varpi = \delta\omega_{aux} - \delta\omega_{main} + D_{int}(\mu_{aux})\mu$, where $D_{int}(\mu_{aux})$ is the integrated dispersion of the microresonator at the mode μ_{aux}. As presented in refs. [31,32], this multicolour LLE formalism allows for straightforward understanding of the DW phase-matching conditions, as any phase matching with the second colour will occur at the zero crossing of $D_{int}(\mu) + \delta\omega_{aux}$, allowing for the creation of a synthetic DW. For the geometry we study in the experiments presented later, higher-order dispersion is present, resulting in a roll-off in D_{int} with an eventual zero crossing and generation of a DKS DW. We auxiliary pump away from the DKS DW, with the higher-order dispersion providing a phase-matching point that is on the same side of the main pump (Fig. 2a).

We simulate the multicolour LLE system with a main pump at $\mu = 0$, an auxiliary pump at $\mu_{aux} = -90$ and the dispersion profile presented in Fig. 2a. We introduce the reference laser that triggers the synchronization through the inclusion in equation (2) of an additional driving force $\sqrt{\kappa_{ext}P_{ref}}\exp(i\Omega t + i\mu_{ref}\theta)$, with $\Omega = \delta\omega_{ref} - \delta\omega_{main} + D_{int}(\mu_{ref}) - \varpi$ the frequency offset between the reference and the closest secondary comb tooth, with $\delta\omega_{ref}$ the reference pump detuning, and $\mu_{ref} = -45$ being the mode (relative to the main pump) at which we send the reference pump. We adiabatically and linearly sweep the detuning of the reference pump while seeding the initial solution with the soliton and secondary colour solution for $a_{dks}(\theta, t = 0)$ and $a_{sec}(\theta, t = 0)$, respectively, and keeping both the main and the auxiliary pump fixed.

When out of synchronization, the simulation highlights that the auxiliary and DKS colours travel at the same group velocity (Fig. 2c,d) as the DKS drifts in θ at the same rate as the secondary colour. Once the reference laser is within the KIS bandwidth, it captures the secondary colour comb tooth, stretching or compressing the microcomb and changing the secondary colour repetition rate (Fig. 2b) with a slope given by the OFD factor set by $\Delta\mu = \mu_{ref} - \mu_{aux} = 45$, and hence controlling its group velocity. Because of the XPM binding, the DKS must follow any variation of group velocity imprinted onto the secondary colour, which is apparent using the two-wave LLE formalism as they drift together. Hence, even if the synchronization is performed on the secondary colour, the DKS repetition rate can be controlled. We can compare this scheme against a direct KIS at the same mode μ_{ref}, where the DKS comb does not present any DW and its shape closely follows a sech^2 spectral envelope. Indeed, the KIS bandwidth $\Delta\omega_{kis} = 2\omega_{rep}|\Delta\mu|E_{kis}$, with $E_{kis} = \sqrt{\frac{\kappa_{ext}}{\kappa^2}P_{ref}|A_X(\mu_{ref})|^2}/E_X$ and E_X and $A_X(\mu_{ref})$ being the total energy and the energy of the comb tooth at mode μ_{ref} with X the soliton or secondary colour, and is directly proportional to the energy of the synchronization mode. Hence, for a fair comparison, all the resonator parameters, such as the resonator free spectral range D_1, κ and κ_{ext}, must remain the same. In addition, we have chosen this particular configuration as it conveniently results in the same OFD factor $\Delta\mu$ for the direct and colour KIS, with only a change of sign changing the direction of the DKS repetition rate ω_{rep} trend against reference pump detuning. In the direct-KIS scenario, the available comb tooth energy $|A_{sec}(\mu_{ref})|^2$ is considerably lower, by about 17 dB compared with the synthetic DW. In addition, the intracavity reference pump does not experience resonance enhancement (and could be considered single pass) due to the close to 40 GHz offset of the comb and its nearest cavity mode—with assumed losses resulting in an offset of more than 40 resonance linewidths—preventing any substantial resonant power build-up. This translates to a KIS bandwidth about 10× smaller than the colour-KIS bandwidth, with 130 MHz and 1.53 GHz synchronization bandwidths, respectively (Fig. 2b).

Experimental nonlinear characterization of the microring

Experimentally, we use a Si$_3$N$_4$ microring with a nominal thickness of $H = 670$ nm embedded in silicon dioxide (SiO$_2$) and a designed ring
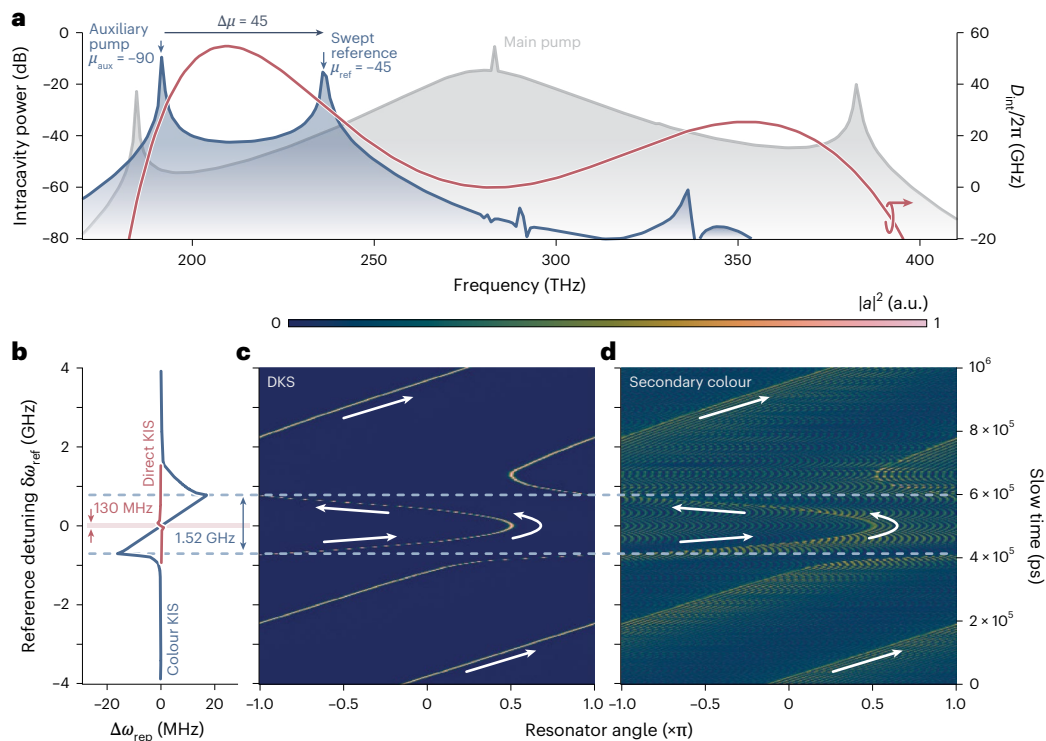
Fig. 2 | Theoretical study of the colour-KIS effect. a, Two-wave LLE simulation results for the DKS (grey) and secondary colour (blue), using the dispersion profile similar to experimental system (red, right scale). The auxiliary pump is held fixed and on-resonance at $\mu = -90$. The reference pump, which is injected at the (high frequency) second-colour DW, is adiabatically swept. The power is normalized to 1 mW. **b**, Repetition rate variation of the DKS $\Delta\omega_{rep}$ against time, with a linear ramp of the reference pump detuning $\delta\omega_{ref}$. Once close enough to the secondary colour comb tooth, the reference pump grabs it and modifies the secondary colour repetition rate ω_{rep} (blue). Through XPM, the DKS repetition rate is also modified. We compare it against direct KIS at the same mode $\mu_{ref} = -45$ (red), resulting in an opposite ω_{rep} slope, with a KIS bandwidth about 10× smaller than the colour-KIS bandwidth with the same reference pump

power. The detuning $\delta\omega_{ref}$ in both cases is normalized such that a null repetition rate variation while synchronized corresponds to the same repetition rate when outside the synchronization regime. **c,d**, Evolution of the DKS (**c**) and secondary colour (**d**) in the resonator angle against the slow time t (where about 1 ps corresponds to 1 soliton round trip), hence the reference detuning. Their trajectories (white arrows) follow the same path as their group velocities are bound, even when the synchronization occurs at the secondary colour. Outside of the colour KIS, their drift in the slow time t is the same highlighting the absence of impact of the reference onto the soliton group velocity. In the second-colour synchronization regime, the drift becomes dependent with the reference detuning, hence, colour KIS provides a means to change the DKS repetition rate.

width of RW = 890 nm, presenting a similar dispersion profile (Fig. 3a) to the one used in the simulations in Fig. 2. The DKS is obtained by pumping the ring at 283 THz with about 150 mW on-chip power, while the introduction of an auxiliary pump of about 2 mW in the 230 THz band or the 190 THz band creates only a secondary colour without disturbing the DKS comb (Fig. 3b). It is apparent that no direct KIS could occur between the DKS and the secondary colour as the two comb components are separated by about 40 GHz (resolved with an optical spectrum analyser; Fig. 3b, left inset). We further verify the flexibility and efficiency of the creation of new synthetic DWs by auxiliary pumping different modes in the 190 THz band and the 230 THz band. Figure 3c,d highlights the creation of a new DW in these other laser bands, and how the synthetic DW spectral position, which will determine where the KIS reference laser is applied, can be flexibly controlled by tuning the auxiliary laser frequency. A significant improvement of 25 dB (190 THz band auxiliary pump) or 32 dB (230 THz band auxiliary pump) of the comb tooth power available at the new DW where the colour KIS will happen is observed compared with the nearest DKS comb tooth. Along with the possibility to send the reference on-resonance, it confirms the theoretical investigation previously conducted that colour KIS will be more efficient than conducting a direct KIS at these modes, as the colour-KIS energy will be about 30× larger than the one for direct KIS, and we were not able to observe direct KIS at these modes of interest between $\mu = -51$ and $\mu = -60$.

DKS repetition rate entrainment from colour KIS

To characterize the colour KIS, we measure at the same time the repetition rate ω_{rep} and the frequency offset between the reference laser and the secondary colour Ω (see experimental set-up in the Supplementary Section 1). As our focus is on DKS repetition rate control, the repetition rate of the system is measured only at the DKS colour. This is done by measurement around 272 THz, where the secondary colour presents negligible power compared with the DKS, as evident through a comparison of the spectra with and without the auxiliary/reference pumps (Fig. 3b).

First, we use the 190 THz continuously tunable laser (CTL) as the auxiliary pump generating the secondary colour, and keep its detuning fixed. We use the 230 THz CTL to act as the reference and it is frequency swept close to the secondary colour comb tooth (Fig. 4a). We use the different modes that have been presented in Fig. 3c,d, resulting in a variation of $\Delta\mu = 25$ to $\Delta\mu = 41$. A clear change in the repetition rate following a linear trend with the reference detuning occurs when Ω is locked to zero, consistent with conventional KIS behaviour, except in these measurements $\Omega = 0$ corresponds to a phase locking at the second colour while the measurement of the repetition rate variation $\Delta\omega_{rep}$ is at the DKS colour, highlighting the XPM interplay linking the colour KIS to the DKS. We verify the linear trend of the repetition rate entrainment by overlaying the reference laser detuning divided by $\Delta\mu$, which closely matches $\Delta\omega_{rep}$. We note here that this linear trend is plotted without offset or scaling, as the zero detuning is accurately
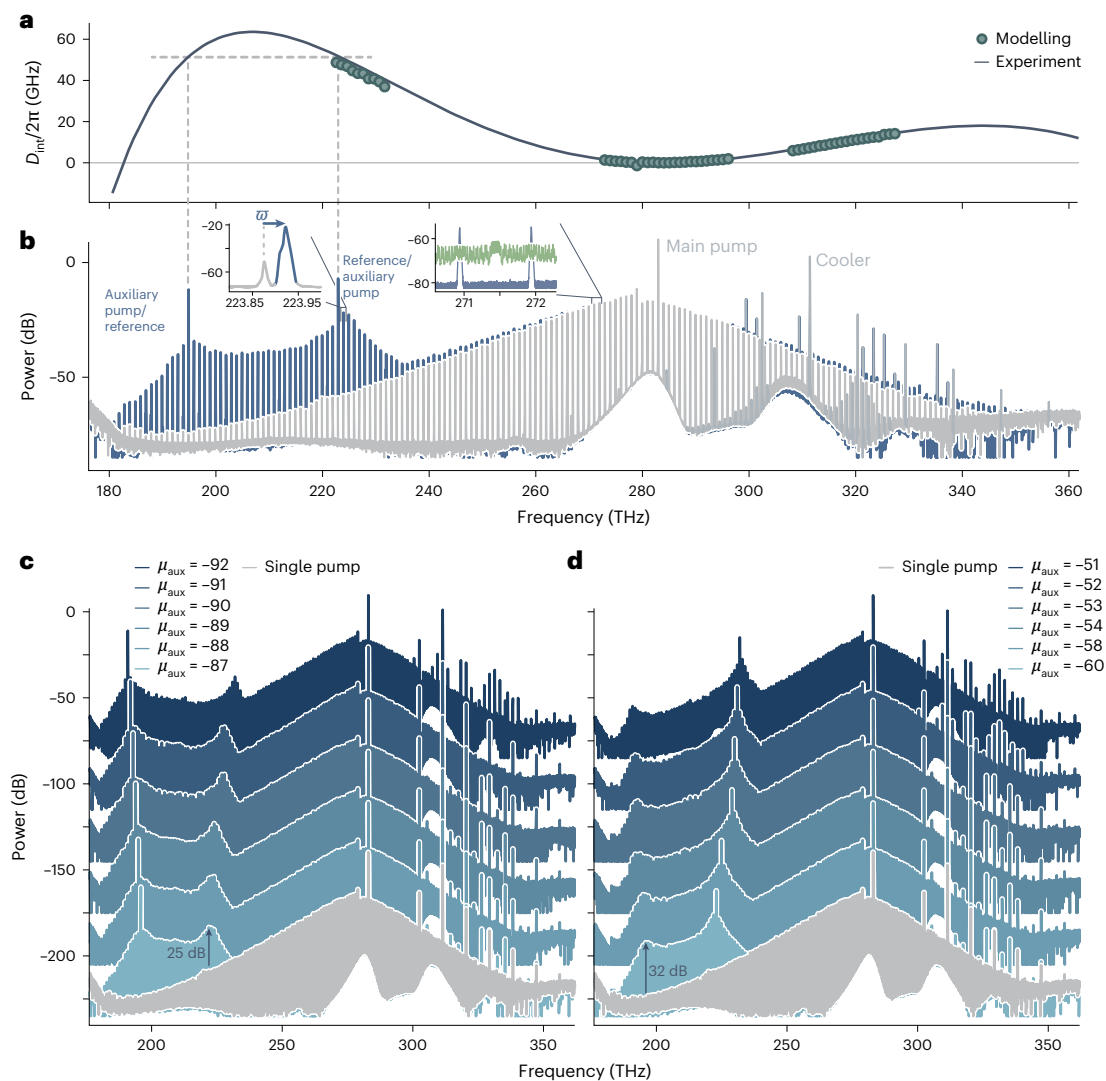
Fig. 3 | DKS and new DW generated via auxiliary pumping. a, Integrated dispersion from wavemeter-calibrated resonance frequencies (50 MHz uncertainty, within marker size) measurement of the fundamental transverse-electric mode (circles) and from the finite-element method dispersion modelling (solid line), showcasing close agreement and used in Fig. 2. The phase matching with the auxiliary pump for where creation of a new synthetic DW appears is shown by the grey dashed line. **b**, Single-pumped DKS microcomb spectrum (grey) obtained using the counter-propagative cooler method[27,35]. The secondary colour (blue) is generated by the auxiliary pump, creating a new synthetic DW where the reference pump can be sent to trigger the colour KIS. The DKS and secondary colour are offset from each other by about ϖ = +40 GHz (left inset; the grey comb line is present in either the single pump or auxiliary pump case, while the blue comb line originates from the auxiliary pump), in accordance with the integrated dispersion value at the auxiliary pump. For subsequent measurements in Fig. 4, we measure the repetition rate of only the DKS using an electro-optic comb apparatus that modulates two adjacent DKS comb teeth (right inset; green is the electro-optically modulated spectrum). The power is normalized to 1 mW. **c,d** Optical spectra for different auxiliary pumped modes in the 190 THz band (**c**) and the 230 THz band (**d**). Compared with the single-pumped DKS (grey), the available comb tooth power for KIS is increased by 25 dB (**c**) and 32 dB (**d**).

calibrated using the technique presented in the Supplementary Section 2 and since the OFD factor is a simple comb tooth counting. In addition, we note a discrepancy in KIS bandwidth between the simulation presented in Fig. 2 and the experimental result. This is probably a result of resonator–waveguide coupling dispersion that leads to a non-trivial variation of κ_{ext} and E, and which is not included in the LLE model. We can then switch the system, where the 230 THz CTL becomes the fixed auxiliary pump creating the secondary colour while the 190 THz CTL becomes the swept reference pump (Fig. 4b). Similar results as previously described are obtained, yet this time the OFD coefficient $\Delta\mu = \mu_{ref} - \mu_{aux}$ is negative. The repetition rate entrainment slope becomes negative when $\Omega = 0$, and is once again accurately captured by a simple linear trend accounting for $1/\Delta\mu$. We note that this experiment has been conducted while maintaining the same exact DKS state, highlighting the little impact the secondary colour and its

synchronization has on the stability of the DKS, further providing flexibility to the system for on-the-fly reconfigurable OFD.

DKS repetition rate phase noise from colour KIS

We investigate the phase noise of the DKS repetition rate while the second colour becomes synchronized. For the different OFD factors presented in Fig. 4, we enter the colour-KIS regime and lock both auxiliary and reference lasers to independent fibre Mach–Zehnder interferometers with a 10 MHz free spectral range, while the main pump and cooler pump are free running. Using a third similar Mach–Zehnder interferometer with a 40 MHz free spectral range, we measure the optical phase noise of both pump lasers. We note that in this measurement we account for the noise of both lasers; however, as the 230 THz laser carries larger phase noise while locked than the 190 THz laser (Supplementary Section 3), only accounting for the former to compare
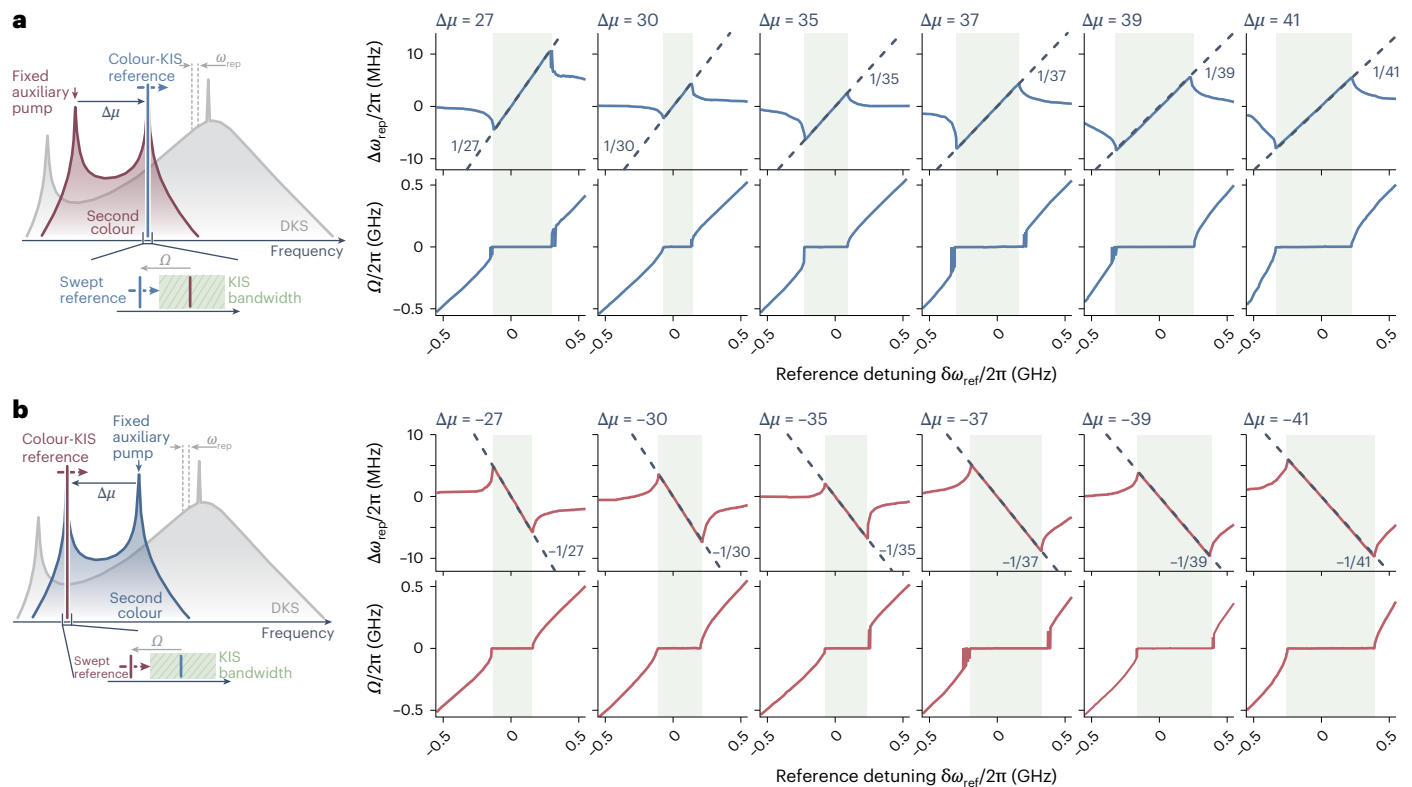
Fig. 4 | Repetition rate control and OFD through colour KIS. Characterization of the repetition rate entrainment (top) and beat note between the reference and secondary colour (bottom) for different mode spacing $\Delta\mu$ between auxiliary and reference pumps, corresponding to the different auxiliary pumping presented in Fig. 3. The repetition rate ω_{rep} is measured at only the DKS. Both $\Delta\omega_{rep}$ and Ω are extracted from simultaneous temporal measurement and calibrated according to Supplementary Section 2. The colour-KIS regime is highlighted by the green area, where a linear change of ω_{rep} following the $\Delta\mu$ OFD factor is observed

(dashed lines). We emphasize that this trend is neither offset nor scaled owing to accurate measurement of the zero detuning. Simultaneously, Ω is locked to zero and hence the reference pump is capturing its nearest secondary colour comb tooth. **a**, Measurements in the case of a fixed auxiliary pump in the 190 THz band and a swept reference pump in the 230 THz range. **b**, Measurements in the case of a fixed auxiliary pump in the 230 THz band and a swept reference pump in the 190 THz range. The change in sign of the slope of $\Delta\omega_{rep}$ within the colour-KIS window between **a** and **b** is consistent with the change in sign of $\Delta\mu$.

against ω_{rep} phase noise enables verification of OFD. For each value of $\Delta\mu$, the repetition rate is well matched to the laser phase noise divided by the OFD factor $\Delta\mu^2$ (Fig. 5). Although the repetition rate entrainment presented in Fig. 4 already demonstrated OFD based on the colour-KIS technique, these additional phase noise measurements highlight that the XPM-mediated transfer of synchronization of the second colour onto the DKS does not carry additional noise, so that colour KIS can be used to stabilize a DKS repetition rate indirectly. We further note that for $\Delta\mu = 30$, we have swept the reference pump over a range of about 120 MHz at a 75 Hz rate following a triangular waveform, and confirmed that no additional noise is present in the repetition rate phase noise. This is consistent with ω_{rep} being locked for both colours, while the frequency offset between the two combs is not. Essentially, while in the colour-KIS regime, all of the phase noise of the main pump is transferred onto the CEO noise of the DKS.

Large tunability of colour-KIS frequency

Finally, we address the large tunability that the colour KIS enables. In contrast to the standard KIS scheme, the colour KIS does not occur on the fixed-frequency markers defined by the repetition rate and the main pump (that is, the CEO frequency). Instead, the secondary colours live at a CEO offset from the main pump, which can be widely tuned through mode hopping between cavity resonances, as previously demonstrated (Fig. 3c,d). In addition, a finer tuning of the CEO frequency offset of the second colour can be obtained through auxiliary pump detuning from its resonance, resulting in the tuning of the synthetic DW[29]. In particular, as the quality factor and coupling regime requirements

are much less stringent than for DKS generation, one can harness the natural overcoupling at lower frequencies than the main pump from straight-waveguide coupling[33], resulting in large secondary colour CEO offset tunability while still dropping significant auxiliary power from the waveguide to the cavity. The repetition rate of the DKS remaining mostly unperturbed with the auxiliary pump detuning enables one to tune the secondary colour comb tooth at which the colour KIS occurs. We demonstrate this effect experimentally using a OFD factor $\Delta\mu = 34$ between the auxiliary and reference pump in the same DKS presented previously (Fig. 6). The reference laser is swept, similarly to Fig. 4, while the auxiliary pump is fixed. The detuning of the auxiliary pump $\delta\omega_{aux}$ enables all the comb teeth of the secondary colour to also be shifted by $\delta\omega_{aux}$, thus shifting the colour-KIS window accordingly. We demonstrate a tuning of over 10 GHz of the KIS window with about 5 mW of on-chip power for both pumps, respectively, corresponding to a tunability of about 10× the optimized colour-KIS bandwidth at this power when both pumps are at the centre of their respective resonances. This tunability is limited by only the available power of the auxiliary pump, and could be further increased by using a more powerful laser while remaining in the thermal stability range of the DKS. Such tunability is a key feature of the colour-KIS scheme, as it enables synchronization to occur at a precise target frequency, for instance, to match a fixed-frequency ultrastable laser.
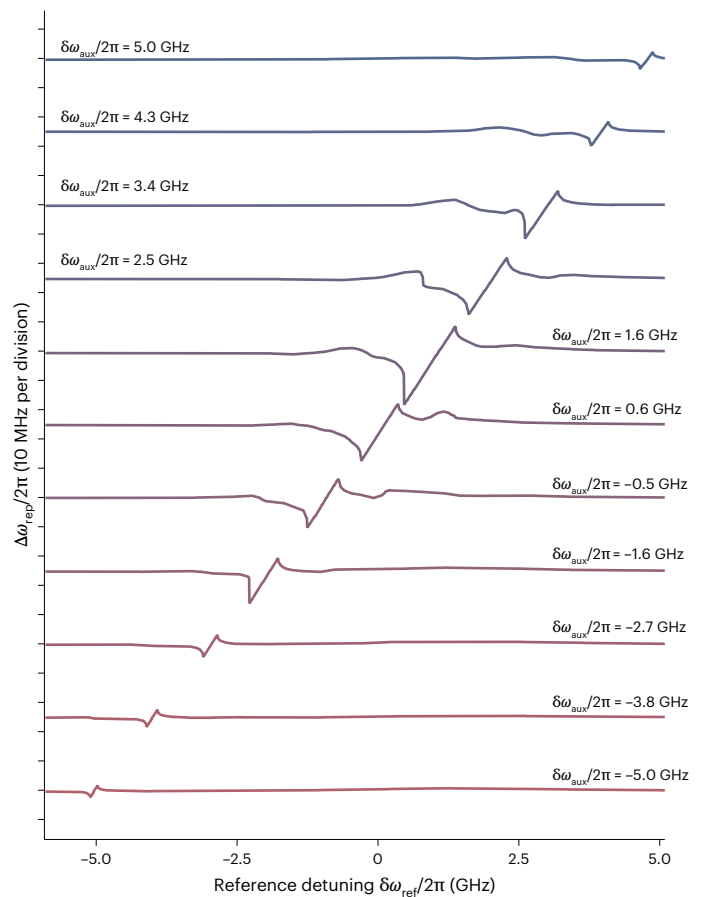
Discussion

In conclusion, we have demonstrated a way to efficiently access the KIS regime, enabling cavity soliton repetition rate control and OFD with
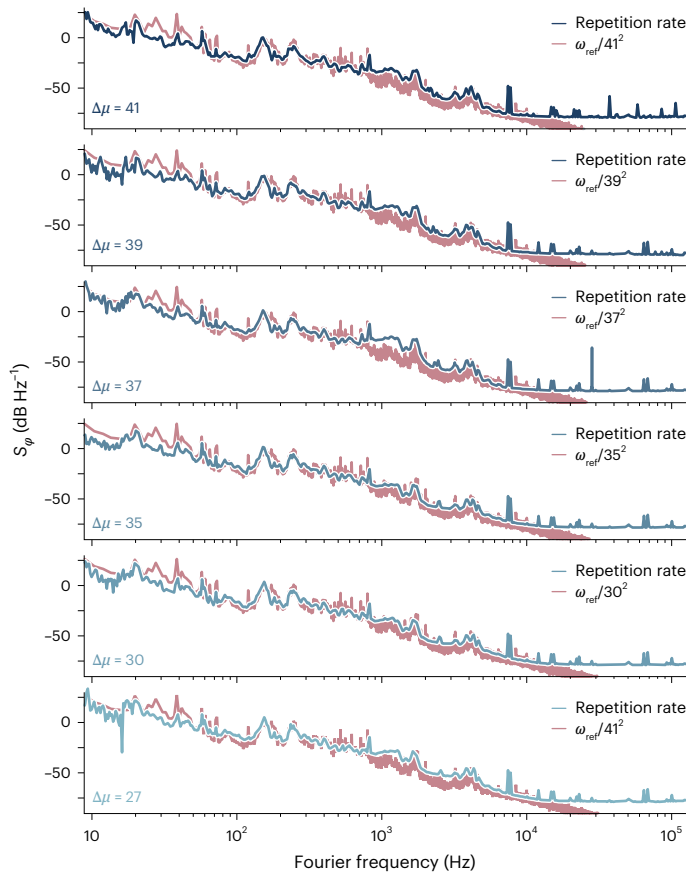
Fig. 5 | Colour-KIS noise OFD onto the DKS repetition rate. OFD characterization of the repetition rate phase noise S_φ for different values of $\Delta\mu$. The auxiliary laser and reference laser are both locked to separate 10 MHz free spectral range Mach–Zehnder interferometers, with the 230 THz range CTL carrying most of the optical noise. Once divided by the appropriate OFD factor $\Delta\mu^2$, the laser phase noise (shown in red) overlaps with the DKS ω_{rep} phase noise (shown in dark blue to light blue for decreasing $\Delta\mu$) according to the KIS principle. Here the stability of the DKS repetition rate comes from KIS of ω_{rep} of the secondary colour, which is then transferred to the DKS ω_{rep} through XPM. The power is referenced to that of the carrier, namely, dBc Hz^{-1}.

Fig. 6 | Tunability of the secondary colour comb tooth for colour-KIS frequency versatility. Using the same DKS previously presented, we sweep the reference laser around 226 THz while the auxiliary pump is parked around the cavity mode at 192 THz, leading to an OFD factor $\Delta\mu = 34$ consistent with the $\Delta\omega_{rep}$ entrainment slope against the reference detuning $\delta\omega_{ref}$. The auxiliary pump detuning $\delta\omega_{aux}/2\pi$ is tuned in steps over 10 GHz and the colour-KIS frequency window is tuned accordingly, demonstrating the possibility to match a precise target frequency at which the synchronization shall happen.

all-optical synchronization of the comb. Using the fundamental group velocity binding between a DKS colour and a secondary colour created by an auxiliary laser travelling in the same microring resonator, we create phase-matching conditions that enable new synthetic DWs that can be used for synchronization, and whose spectral locations can be flexibly tuned. Compared with synchronization to a reference laser at the same frequency using a single-pumped DKS, the comb tooth power is orders of magnitude larger while providing on-resonance operation for the reference laser to efficiently transfer its power inside the resonator. We show theoretically that the KIS bandwidth for a similar situation between direct and colour KIS is increased by at least an order of magnitude. Experimentally, we have demonstrated this effect using an integrated microring resonator, where repetition rate entrainment according to the OFD factor between the auxiliary and the reference pump is verified. The spectral separation between the auxiliary and reference pump, and hence the division factor, can be widely controlled with respect to the underlying cavity dispersion without disrupting the stability of the DKS. We also show that the locking of the group velocity of the second colour through auxiliary and reference pump locking in the colour-KIS regime is transferred onto the DKS repetition rate in a noiseless fashion, despite the indirect control of the DKS through the XPM-coupled secondary colour. Finally, we have demonstrated the versatility of the colour-KIS approach compared with the standard KIS

one, where the synchronization frequency (and window) can be largely tuned without impacting the DKS. Our work enables an efficient way to control the large repetition rate of integrated microresonator combs, in particular in situations where the cavity dispersion could otherwise prevent direct KIS.

We further discuss a few important implications of the colour-KIS effect. For example, KIS-enabled OFD has recently been shown in the context of low-noise microwave generation with a greatly simplified architecture[21]. Our colour-KIS scheme enables further important simplifications. Indeed, it is interesting to note that the main pump does not have a role in the repetition rate control and stabilization as the CEO offset between colours ϖ is unlocked and therefore uncoupled from the OFD approach. This enables the main pump to be freely tuned as needed to generate the DKS, without further conditions on its stability. In addition, although we have mostly focused on demonstrating the control of the single repetition rate of the different colours, it is important to point out that the secondary colour forms its own frequency comb whose repetition rate can also be detected and stabilized. As a result, the colour-KIS scheme brings the possibility to coherently phase lock an auxiliary laser to an ultranarrow-linewidth laser, through the repetition rate feedback onto the auxiliary laser. As noted above, in colour KIS, such a scheme is independent of the main pump; indeed, the main DKS essentially acts as an intermediary whose XPM interactions with the second colour enable a single group velocity to exist.

We note that while thus far colour KIS has required an additional laser compared with direct KIS, one could leverage the cooler pump to also act as the auxiliary pump that creates the synthetic DW. This simplification of the colour-KIS architecture is still effective when the auxiliary pump is counter-propagating, similar to the synchronization of two counter-propagating solitons[34], and is demonstrated in Supplementary Section 4. Finally, the creation of synthetic DWs can be extended to other colours, which has been demonstrated to expand the comb bandwidth well beyond an octave[26], and hence the colour-KIS scheme may find application in the stabilization of such ultrabroadband integrated frequency combs. Beyond the above, our work could find direct application in distance ranging while enabling new techniques for fundamental studies of DKS dynamics in micrometre-scale resonators.

Online content

Any methods, additional references, Nature Portfolio reporting summaries, source data, extended data, supplementary information, acknowledgements, peer review information; details of author contributions and competing interests; and statements of data and code availability are available at https://doi.org/10.1038/s41566-024-01540-w.

References

1. Fortier, T. & Baumann, E. 20 years of developments in optical frequency comb technology and applications. *Commun. Phys.* **2**, 153 (2019).
2. Diddams, S. A., Vahala, K. & Udem, T. Optical frequency combs: coherently uniting the electromagnetic spectrum. *Science* **369**, eaay3676 (2020).
3. Spencer, D. T. et al. An optical-frequency synthesizer using integrated photonics. *Nature* **557**, 81–85 (2018).
4. Newman, Z. L. et al. Architecture for the photonic integration of an optical atomic clock. *Optica* **6**, 680 (2019).
5. Oelker, E. et al. Demonstration of 4.8×10^{-17} stability at 1 s for two independent optical clocks. *Nat. Photon.* **13**, 714–719 (2019).
6. Giorgetta, F. R. et al. Optical two-way time and frequency transfer over free space. *Nat. Photon.* **7**, 434–438 (2013).
7. Caldwell, E. D. et al. Quantum-limited optical time transfer for future geosynchronous links. *Nature* **618**, 721–726 (2023).
8. Tetsumoto, T. et al. Optically referenced 300 GHz millimetre-wave oscillator. *Nat. Photon.* **15**, 516–522 (2021).
9. Xie, X. et al. Photonic microwave signals with zeptosecond-level absolute timing noise. *Nat. Photon.* **11**, 44–47 (2017).
10. Riemensberger, J. et al. Massively parallel coherent laser ranging using a soliton microcomb. *Nature* **581**, 164–170 (2020).
11. Kippenberg, T. J., Gaeta, A. L., Lipson, M. & Gorodetsky, M. L. Dissipative Kerr solitons in optical microresonators. *Science* **361**, eaan8083 (2018).
12. Liu, J. et al. High-yield, wafer-scale fabrication of ultralow-loss, dispersion-engineered silicon nitride photonic circuits. *Nat. Commun.* **12**, 2236 (2021).
13. Wildi, T., Gaafar, M. A., Voumard, T., Ludwig, M. & Herr, T. Dissipative Kerr solitons in integrated Fabry–Perot microresonators. *Optica* **10**, 650–656 (2023).
14. Stern, B., Ji, X., Okawachi, Y., Gaeta, A. L. & Lipson, M. Battery-operated integrated frequency comb generator. *Nature* **562**, 401–405 (2018).
15. Fortier, T. M. et al. Generation of ultrastable microwaves via optical frequency division. *Nat. Photon.* **5**, 425–429 (2011).
16. Liu, K. et al. 36 Hz integral linewidth laser based on a photonic integrated 4.0 m coil resonator. *Optica* **9**, 770–775 (2022).
17. Kudelin, I. et al. Photonic chip-based low-noise microwave oscillator. *Nature* **627**, 534–539 (2024).
18. Sun, S. et al. Integrated optical frequency division for microwave and mmWave generation. *Nature* **627**, 540–545 (2024).
19. Moille, G. et al. Kerr-induced synchronization of a cavity soliton to an optical reference. *Nature* **624**, 267–274 (2023).
20. Wildi, T., Ulanov, A., Englebert, N., Voumard, T. & Herr, T. Sideband injection locking in microresonator frequency combs. *APL Photon.* **8**, 120801 (2023).
21. Sun, S. et al. Kerr optical frequency division with integrated photonics for stable microwave and mmWave generation. Preprint at https://arxiv.org/abs/2402.11772v1 (2024).
22. Moille, G. et al. *Frontiers in Optics and Laser Science* Report No. FTh3E-2 (Optica Publishing Group, 2023).
23. Shen, B. et al. Integrated turnkey soliton microcombs. *Nature* **582**, 365–369 (2020).
24. Ulanov, A. E. et al. Synthetic reflection self-injection-locked microcombs. *Nat. Photon.* **18**, 294–299 (2024).
25. Voloshin, A. S. et al. Dynamics of soliton self-injection locking in optical microresonators. *Nat. Commun.* **12**, 235 (2021).
26. Moille, G. et al. Ultra-broadband Kerr microcomb through soliton spectral translation. *Nat. Commun.* **12**, 7275 (2021).
27. Zhang, S., Silver, J. M., Bi, T. & Del'Haye, P. Spectral extension and synchronization of microcombs in a single microresonator. *Nat. Commun.* **11**, 6384 (2020).
28. Wang, Y. et al. Universal mechanism for the binding of temporal cavity solitons. *Optica* **4**, 855 (2017).
29. Qureshi, P. C. et al. Soliton linear-wave scattering in a Kerr microresonator. *Commun. Phys.* **5**, 123 (2022).
30. Taheri, H., Matsko, A. B. & Maleki, L. Optical lattice trap for Kerr solitons. *Eur. Phys. J. D* **71**, 153 (2017).
31. Moille, G. et al. Two-dimensional nonlinear mixing between a dissipative Kerr soliton and continuous waves for a higher-dimension frequency comb. Preprint at https://arxiv.org/abs/2303.10026 (2023).
32. Shandilya, P. H., Moille, G., D'Aguanno, G., Srinivasan, K. & Menyuk, C. R. *Frontiers in Optics and Laser Science* Report No. JW4A-48 (Optica Publishing Group, 2023).
33. Moille, G. et al. Broadband resonator–waveguide coupling for efficient extraction of octave-spanning microcombs. *Opt. Lett.* **44**, 4737 (2019).
34. Yang, Q.-F., Yi, X., Yang, K. Y. & Vahala, K. Counter-propagating solitons in microresonators. *Nat. Photon.* **11**, 560–564 (2017).
35. Zhou, H. et al. Soliton bursts and deterministic dissipative Kerr soliton generation in auxiliary-assisted microcavities. *Light Sci. Appl.* **8**, 50 (2019).

Methods

Derivation of the coupled LLE formalism

We start with the multi-pumped LLE (MLLE) with two driving forces as presented in ref. 30

$$
\begin{aligned}
\frac{\partial a}{\partial t} = &\left(-\frac{\kappa}{2} + \mathrm{i}\delta\omega_{\mathrm{main}}\right)a \\
&+ \mathrm{i}\sum_{\mu} D_{\mathrm{int}}(\mu)A\mathrm{e}^{\mathrm{i}\mu\theta} - \mathrm{i}\gamma L|a|^2 a \\
&+ \mathrm{i}\sqrt{\kappa_{\mathrm{ext}}P_{\mathrm{main}}} \\
&+ \mathrm{i}\sqrt{\kappa_{\mathrm{ext}}P_{\mathrm{aux}}}\mathrm{e}^{\mathrm{i}(\delta\omega_{\mathrm{main}}-\delta\omega_{\mathrm{aux}}+D_{\mathrm{int}}(\mu_{\mathrm{aux}}))t+\mathrm{i}\mu_{\mathrm{aux}}\theta}
\end{aligned}
\tag{3}
$$

with $A = \mathrm{FT}[a]$ the azimuthal Fourier transform of a, $\delta\omega_{\mathrm{main}}$ and $\delta\omega_{\mathrm{aux}}$ the detuning of the main and auxiliary pump relative to their mode $\mu = 0$ and $\mu = \mu_{\mathrm{aux}}$, respectively, and $D_{\mathrm{int}}(\mu_{\mathrm{aux}})$ is the integrated dispersion, computed with respect to the main pump, for the auxiliary pumped mode μ_{aux}. Here we have defined the detuning of a pump 'p' with frequency ω_{p} from its nearest cavity resonance frequency $\omega(\mu = \mu_{\mathrm{p}})$ as $\delta\omega_{\mathrm{p}} = \omega(\mu = \mu_{\mathrm{p}}) - \omega_{\mathrm{p}}$. In this notation, $\delta\omega_{\mathrm{p}} > 0$ corresponds to a red-detuned pump. The integrated dispersion is defined as $D_{\mathrm{int}}(\mu) = (\omega_{\mathrm{res}}(\mu) - \omega_{\mathrm{res}}(\mu = 0)) - D_1\mu$, where D_1 is the cavity free spectral range around the main pump resonance and $\omega_{\mathrm{res}}(\mu)$ is the resonance frequency of mode μ. In this formalism of the MLLE, we have assumed that the soliton rotates in the $-\theta$ direction.

We assume that two colours form in the cavity, the second colour experiencing a phase offset $\varpi t = [\delta\omega_{\mathrm{main}} - \delta\omega_{\mathrm{aux}} + D_{\mathrm{int}}(\mu_{\mathrm{aux}})]t$ from the soliton. Therefore a can be written as

$$
a = a_{\mathrm{dks}} + a_{\mathrm{sec}}\mathrm{e}^{\mathrm{i}\varpi t}, \tag{4}
$$

Substituting equation (4) in equation (3) and retaining only the phase-matched terms

$$
\begin{aligned}
\frac{\partial a_{\mathrm{dks}}}{\partial t} + \frac{\partial a_{\mathrm{sec}}}{\partial t}\mathrm{e}^{\mathrm{i}\varpi t} + \mathrm{i}\varpi a_{\mathrm{sec}}\mathrm{e}^{\mathrm{i}\varpi t} = &\left(-\frac{\kappa}{2} + \mathrm{i}\delta\omega_{\mathrm{main}}\right)(a_{\mathrm{dks}} + a_{\mathrm{sec}}\mathrm{e}^{\mathrm{i}\varpi t}) \\
&+ \mathrm{i}\sum_{\mu} D_{\mathrm{int}}(\mu)A_{\mathrm{dks}}\mathrm{e}^{\mathrm{i}\mu\theta} \\
&+ \mathrm{i}\sum_{\mu} D_{\mathrm{int}}(\mu)A_{\mathrm{sec}}(\mu)\mathrm{e}^{\mathrm{i}\mu\theta}\mathrm{e}^{\mathrm{i}\varpi t} \\
&- \mathrm{i}\gamma L\left(|a_{\mathrm{dks}}|^2 + 2|a_{\mathrm{sec}}|^2\right)a_{\mathrm{dks}} \\
&- \mathrm{i}\gamma L\left(|a_{\mathrm{sec}}|^2 + 2|a_{\mathrm{dks}}|^2\right)a_{\mathrm{sec}}\mathrm{e}^{\mathrm{i}\varpi t} \\
&+ \mathrm{i}\sqrt{\kappa_{\mathrm{ext}}P_{\mathrm{main}}} + \mathrm{i}\sqrt{\kappa_{\mathrm{ext}}P_{\mathrm{aux}}}\mathrm{e}^{(\mathrm{i}\varpi t + \mathrm{i}\mu_{\mathrm{aux}}\theta)}
\end{aligned}
\tag{5}
$$

Separating the terms with and without $\mathrm{e}^{\mathrm{i}\varpi t}$, we get the equation for a_{dks}

$$
\begin{aligned}
\frac{\partial a_{\mathrm{dks}}}{\partial t} = &\left(-\frac{\kappa}{2} + \mathrm{i}\delta\omega_{\mathrm{main}}\right)a_{\mathrm{dks}} \\
&+ \mathrm{i}\sum_{\mu} D_{\mathrm{int}}(\mu)a_{\mathrm{dks}}\mathrm{e}^{\mathrm{i}\mu\theta} \\
&- \mathrm{i}\gamma L(|a_{\mathrm{dks}}|^2 + 2|a_{\mathrm{sec}}|^2)a_{\mathrm{dks}} \\
&+ \mathrm{i}\sqrt{\kappa_{\mathrm{ext}}P_{\mathrm{main}}},
\end{aligned}
\tag{6}
$$

which is equation (1) in the main text, and for a

$$
\begin{aligned}
\frac{\partial a_{\mathrm{sec}}}{\partial t} + \mathrm{i}\varpi a_{\mathrm{sec}} = &\left(-\frac{\kappa}{2} + \mathrm{i}\delta\omega_{\mathrm{main}}\right)a_{\mathrm{sec}} \\
&+ \mathrm{i}\sum_{\mu'} D_{\mathrm{int}}(\mu')a_{\mathrm{sec}}(\mu')\mathrm{e}^{\mathrm{i}\mu\theta} \\
&- \mathrm{i}\gamma L(|a_{\mathrm{sec}}|^2 + 2|a_{\mathrm{dks}}|^2)a_{\mathrm{sec}} \\
&+ \mathrm{i}\sqrt{\kappa_{\mathrm{ext}}P_{\mathrm{sec}}}\mathrm{e}^{\mathrm{i}\mu_{\mathrm{aux}}\theta},
\end{aligned}
\tag{7}
$$

Using the definition of $\varpi = \delta\omega_{\mathrm{main}} - \delta\omega_{\mathrm{aux}} + D_{\mathrm{int}}(\mu_{\mathrm{aux}})$ gives

$$
\begin{aligned}
\frac{\partial a_{\mathrm{sec}}}{\partial t} = &\left(-\frac{\kappa}{2} + \mathrm{i}\delta\omega_{\mathrm{aux}} - \mathrm{i}D_{\mathrm{int}}(\mu_{\mathrm{aux}})\right)a_{\mathrm{sec}} \\
&+ \mathrm{i}\sum_{\mu} D_{\mathrm{int}}(\mu)a_{\mathrm{sec}}(\mu)\mathrm{e}^{\mathrm{i}\mu\theta} \\
&- \mathrm{i}\gamma L\left(|a_{\mathrm{sec}}|^2 + 2|a_{\mathrm{dks}}|^2\right)a_{\mathrm{sec}} \\
&+ \mathrm{i}\sqrt{\kappa_{\mathrm{ext}}P_{\mathrm{aux}}}\mathrm{e}^{\mathrm{i}\mu_{\mathrm{aux}}\theta},
\end{aligned}
\tag{8}
$$

Now, we can add a reference pump intended to synchronize the second colour to the MLLE as

$$
\begin{aligned}
\frac{\partial a}{\partial t} = &\left(-\frac{\kappa}{2} + \mathrm{i}\delta\omega_{\mathrm{main}}\right)a \\
&+ \mathrm{i}\sum_{\mu} D_{\mathrm{int}}(\mu)A\mathrm{e}^{\mathrm{i}\mu\theta} - \mathrm{i}\gamma L|a|^2 a + \mathrm{i}\sqrt{\kappa_{\mathrm{ext}}P_{\mathrm{main}}} \\
&+ \mathrm{i}\sqrt{\kappa_{\mathrm{ext}}P_{\mathrm{aux}}}\mathrm{e}^{\mathrm{i}(\delta\omega_{\mathrm{main}}-\delta\omega_{\mathrm{aux}}+D_{\mathrm{int}}(\mu_{\mathrm{aux}}))t+\mathrm{i}\mu_{\mathrm{aux}}\theta} \\
&+ \mathrm{i}\sqrt{\kappa_{\mathrm{ext}}P_{\mathrm{ref}}}\mathrm{e}^{\mathrm{i}(\delta\omega_{\mathrm{main}}-\delta\omega_{\mathrm{ref}}+D_{\mathrm{int}}(\mu_{\mathrm{ref}}))t+\mathrm{i}\mu_{\mathrm{ref}}\theta}
\end{aligned}
\tag{9}
$$

Substituting the solution and separating the equations like before while grouping the reference pump with the equation for the second colour, the coupled LLE for a_{dks} remains unchanged, while a grouped with the reference pump becomes

$$
\begin{aligned}
\frac{\partial a_{\mathrm{sec}}}{\partial t} = &\left(-\frac{\kappa}{2} + \mathrm{i}\delta\omega_{\mathrm{aux}} - \mathrm{i}D_{\mathrm{int}}(\mu_{\mathrm{aux}})\right)a_{\mathrm{sec}} \\
&+ \mathrm{i}\sum_{\mu} D_{\mathrm{int}}(\mu)A_{\mathrm{sec}}(\mu)\mathrm{e}^{\mathrm{i}\mu\theta} \\
&- \mathrm{i}\gamma L\left(|a_{\mathrm{sec}}|^2 + 2|a_{\mathrm{dks}}|^2\right)a_{\mathrm{sec}} \\
&+ \mathrm{i}\sqrt{\kappa_{\mathrm{ext}}P_{\mathrm{aux}}}\mathrm{e}^{\mathrm{i}\mu_{\mathrm{aux}}\theta} \\
&+ \mathrm{i}\sqrt{\kappa_{\mathrm{ext}}P_{\mathrm{ref}}}\mathrm{e}^{\mathrm{i}[\delta\omega_{\mathrm{aux}}-\delta\omega_{\mathrm{ref}}+D_{\mathrm{int}}(\mu_{\mathrm{ref}})-D_{\mathrm{int}}(\mu_{\mathrm{aux}})]t+\mathrm{i}\mu_{\mathrm{ref}}\theta},
\end{aligned}
\tag{10}
$$

With the definition of $\varpi = \delta\omega_{\mathrm{main}} - \delta\omega_{\mathrm{aux}} + D_{\mathrm{int}}(\mu_{\mathrm{aux}})$ as the offset of the secondary colour field relative to the DKS, one can define $\Omega = \delta\omega_{\mathrm{main}} - \delta\omega_{\mathrm{ref}} + D_{\mathrm{int}}(\mu_{\mathrm{ref}}) - \varpi$ as the offset of the reference from its nearest secondary comb tooth. We obtain

$$
\begin{aligned}
\frac{\partial a_{\mathrm{sec}}}{\partial t} = &\left(-\frac{\kappa}{2} + \mathrm{i}\delta\omega_{\mathrm{aux}} - \mathrm{i}D_{\mathrm{int}}(\mu_{\mathrm{sec}})\right)a_{\mathrm{sec}} \\
&+ \mathrm{i}\sum_{\mu} D_{\mathrm{int}}(\mu)A_{\mathrm{sec}}(\mu)\mathrm{e}^{\mathrm{i}\mu\theta} \\
&- \mathrm{i}\gamma L\left(|a_{\mathrm{sec}}|^2 + 2|a_{\mathrm{dks}}|^2\right)a_{\mathrm{sec}} \\
&+ \mathrm{i}\sqrt{\kappa_{\mathrm{ext}}P_{\mathrm{sec}}}\mathrm{e}^{\mathrm{i}\mu_{\mathrm{aux}}\theta} \\
&+ \mathrm{i}\sqrt{\kappa_{\mathrm{ext}}P_{\mathrm{ref}}}\mathrm{e}^{(\mathrm{i}\Omega t+\mathrm{i}\mu_{\mathrm{ref}}\theta)},
\end{aligned}
\tag{11}
$$

which is equation (2) in the main text.

Simulation parameters

In the equations (1) and (2), $\gamma = 2.3\ \mathrm{W}^{-1}\,\mathrm{m}^{-1}$ is the effective nonlinearity calculated at the main pump[19,26], $\kappa/2\pi = 1.1\ \mathrm{GHz}$ is the total loss rate, $\kappa_{\mathrm{ext}} = 1/2\kappa$ is the external coupling rate (that is, $Q_{\mathrm{c}} = Q_{\mathrm{i}} = 500 \times 10^3$ are the coupling and intrinsic quality factors, respectively), $L = 2\pi \times 23\ \mu\mathrm{m}$ is the resonator circumference, and $D_{\mathrm{int}}(\mu)$ is the integrated dispersion accounting for the DKS repetition rate $\omega_{\mathrm{rep}}/2\pi \approx 1\ \mathrm{THz}$.

Resonator design

The photonic chips were fabricated in a commercial foundry in the same fashion as the ones presented in ref. 19. The microring resonator is made of Si_3N_4 embedded in SiO_2. Its dimensions consist of an external ring radius RR = 23 μm, Si_3N_4 thickness of H = 670 nm and ring width of RW = 890 nm. We couple to the ring using a 460-nm-wide waveguide that is at a gap distance from the ring of G = 500 nm. The light is injected through facet coupling with a lensed fibre into the

inverse-taper waveguide that shows a $W = 250$ nm width at the facet. The insertion losses from fibre to chip are approximately 2.3 dB.

Comb generation

The experimental set-up is discussed in detail in Supplementary Section 1. To generate the DKS, we use a 283 THz pump with about 150 mW on-chip power. The DKS is adiabatically accessed using a 308 THz counter-propagating cooler laser that pumps a fundamental transverse-magnetic mode, which thermally stabilizes the resonator and enables long-term operation of the DKS state[36,35]. To generate the secondary colour, we use CTLs spanning between 184 THz and 198 THz with about 2 mW of on-chip power, and 227 THz to 232 THz with about 1 mW of on-chip power. One of these lasers acts as the auxiliary pump that creates the second colour (that is, is fixed), while the other is used as the reference. The higher-order dispersion results in $D_{int}(\mu)$ roll-off, enabling the creation of new synthetic DW phase-matching in the 230 THz range (that is, 1,300 nm range) for auxiliary pumping in the 190 THz range (that is, 1,550 nm range) and vice versa. The experimental dispersion is measured using wavemeter-calibrated resonance frequencies of the first-order transverse-electric mode (Fig. 3a).

Data acquisition method

To measure the repetition rate, we use an electro-optic comb apparatus[19,37] to modulate two adjacent DKS comb teeth and frequency translate $\omega_{rep}/2\pi \approx 1$ THz to a detectable microwave beat note; an example spectrum is shown in the right inset in Fig. 3b. We sweep the reference laser using an electrical ramp signal sent to the CTL piezo element, enabling small detuning to be studied, and measure both ω_{rep} and Ω by recording simultaneously their temporal trace with a fast oscilloscope. We then process these data to create a spectrogram where the temporal dependence of ω_{rep} and Ω are obtained. The detuning calibration is obtained through beating the reference laser against the secondary colour comb tooth while bypassing the resonator (that is, no nonlinearity, hence no synchronization), calibrating the amplitude and the zero of the detuning. For more details, the complete procedure is described in Supplementary Section 2.

Data availability

The data that supports the plots within this paper and other findings of this study are available from the corresponding authors upon request.

Code availability

The simulation code is available from the authors through the pyLLE package available online[38], with a modification that is available upon reasonable request, using the inputs and parameters presented in this work.

References

36. Zhang, S. et al. Sub-milliwatt-level microresonator solitons with extended access range using an auxiliary laser. *Optica* **6**, 206 (2019).

37. Stone, J. R. & Papp, S. B. Harnessing dispersion in soliton microcombs to mitigate thermal noise. *Phys. Rev. Lett.* **125**, 153901 (2020).

38. Moille, G., Li, Q., Xiyuan, L. & Srinivasan, K. pyLLE: a fast and user friendly Lugiato–Lefever equation solver. *J. Res. NIST* **124**, 124012 (2019).

39. Crameri, F. Scientific colour maps. *Zenodo* https://doi.org/10.5281/zenodo.8409685 (2023).

40. Crameri, F., Shephard, G. E. & Heron, P. J. The misuse of colour in science communication. *Nat. Commun.* **11**, 5444 (2020).

Author contributions

G.M. and K.S. led the project. G.M. designed the resonators and performed the measurements and simulations. P.S. and C.M. helped with the theoretical and numerical understanding. A.N. and G.C. helped with the experimental understanding. K.S. helped with data analysis. G.M. and K.S. wrote the paper, with input from all authors. All the authors contributed to and discussed the content of this paper.

Competing interests

G.M., C.M. and K.S have submitted a provisional patent application based on aspects of the work presented in this paper. The other authors declare no competing interests.

Additional information

Supplementary information The online version contains supplementary material available at https://doi.org/10.1038/s41566-024-01540-w.

Correspondence and requests for materials should be addressed to Grégory Moille or Kartik Srinivasan.

Peer review information *Nature Photonics* thanks Mengxi Tan and the other, anonymous, reviewer(s) for their contribution to the peer review of this work.

Reprints and permissions information is available at www.nature.com/reprints.

Versatile optical frequency division with Kerr-induced synchronization at tunable microcomb synthetic dispersive waves
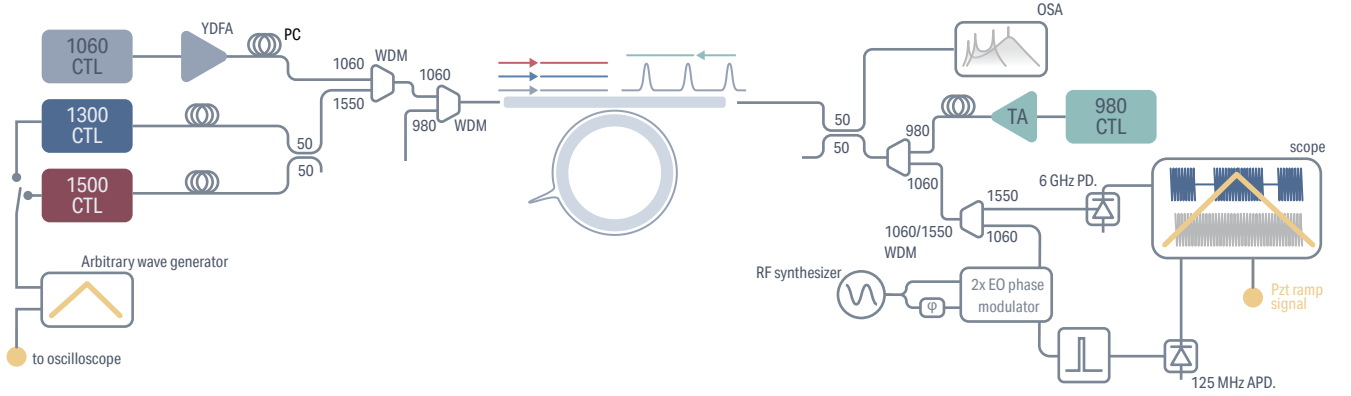
In the format provided by the authors and unedited

# Contents

S.1.   Experimental Setup

Fig. S.1 – **Experimental setup**. A main pump around 283 THz is obtained from an amplified 1060 nm CTL providing about 150 mW of on-chip power to generate a DKS, which is then adiabatically accessed thanks to the amplified and counterpropagating 980 nm CTL cooler pump that thermally stabilizes the resonator. We introduce an auxiliary pump and a reference pump to create the secondary color and trigger the color-KIS with 1300 nm and 1550 nm CTLs. We measure the DKS repetition rate using two cascaded EO phase modulators which we apply to two adjacent Kerr comb lines around 1100 nm. EO-generated sidebands of the two DKS teeth span across the microcomb repetition rate, with high-order sidebands that come close to merging. We filter around this frequency, allowing retrieval of the beat note with a slow ($<$50 MHz bandwidth) APD. The beating between the secondary color and the reference pump is obtained with negligible DKS power thanks to the WDM. Both the repetition rate and the reference beat note are measured in the time domain and then processed and calibrated to obtain the data presented in this work. Other elements such as power meters and photodiodes to verify transmission levels are not displayed to avoid over-complicating the schematic. CTL: continuously tunable laser, YDFA: ytterbium-doped fiber amplifier, TA: tapered amplifier, PC: polarization controller, WDM: wavelength demultiplexer, RF: radiofrequency, OSA: optical spectrum analyzer, PD: photodiode, APD: avalanche photodiode, EO: electro-optic

The experimental setup used in this work is depicted in Fig. S.1. We use a 1060 nm continuously tunable laser (CTL) amplified with an ytterbium-doped fiber amplifier (YDFA) to generate enough power at 283 THz to pump the microring to harness the resonator's third-order nonlinearity. An on-chip power of about 150 mW is sufficient to reach a dissipative Kerr soliton (DKS) state in the fundamental transverse electric mode (TE) of the 23 μm Si_3N_4 microring resonator. To help access this state, we use a 980 nm CTL amplified using a taper amplifier (TA) and set to be counterpropagative and cross-polarized relative to the main pump, so that this cooler pump only thermally stabilizes the resonator for adiabatic access to the DKS [1, 2] while minimizing potential nonlinear mixing with the main pump and/or the DKS. We use a combinations of wavelength demultiplexers (WDMs) at the input and output to avoid any injection of the cooler (main pump) into the main pump (cooler). The auxiliary and reference laser from the 1300 nm and 1550 nm CTLs are injected in the resonator by combining them with the main pump using a WDM, and are also set in the TE polarization. We tap 50 % of the output to probe the microcomb optical spectrum using an optical spectrum analyzer (OSA). We use another WDM at the other 50 % output to separate wavelengths close to 1100 nm, which are electro-optically (EO) modulated at $\Omega_{RF} = 17.87892$ GHz. The EO-generated sidebands of two adjacent DKS comb teeth fill the DKS repetition rate over $N = 56$ EOcomb teeth, providing a measure of the DKS repetition rate $\omega_{rep} = N \times \Omega_{RF} - \delta\omega_{rep} = 1001.21952$ GHz $- \delta\omega_{beat}$ (the minus sign is configuration dependent and has been verified for our experiments), with $\delta\omega_{beat}$ the EOcomb beat note that can be detected by a 50 MHz avalanche photodiode (APD), similar to the methods presented in [3, 4]. The other WDM output is used to measure the beat note Ω between the secondary color and the reference pump. Both signals are processed in the time domain using a high speed oscilloscope. We trigger the scope with the ramp signal used to sweep the piezo element of the CTL, obtaining a temporal trace which can be processed and converted into a spectrogram, enabling instantaneous frequency measurement. The calibration of this technique is further discussed in the next section.

S.2.   Repetition rate and detuning calibrations from temporal traces

The EOcomb beat note $\delta\omega_{beat}$, which directly lets us precisely characterize the repetition rate ω_{rep}, and the reference pump and secondary-color beat Ω are measured in the optical domain using a fast oscilloscope [Fig. S.2a-b], with a temporal resolution of 320 ps. The piezo element is swept at a 50 Hz rate around the detuning of interest. We record simultaneously the temporal trace of $\delta\omega_{beat}$ and Ω, which we process using the scipy.signal.spectrogram python package [5]. We use a binning slice of 30×10^3 points, allowing a frequency resolution of about 104 kHz. The fast Fourier transform (FFT) windowing is performed using a Hanning filter, with an overlap of 10×10^3 points. We obtain
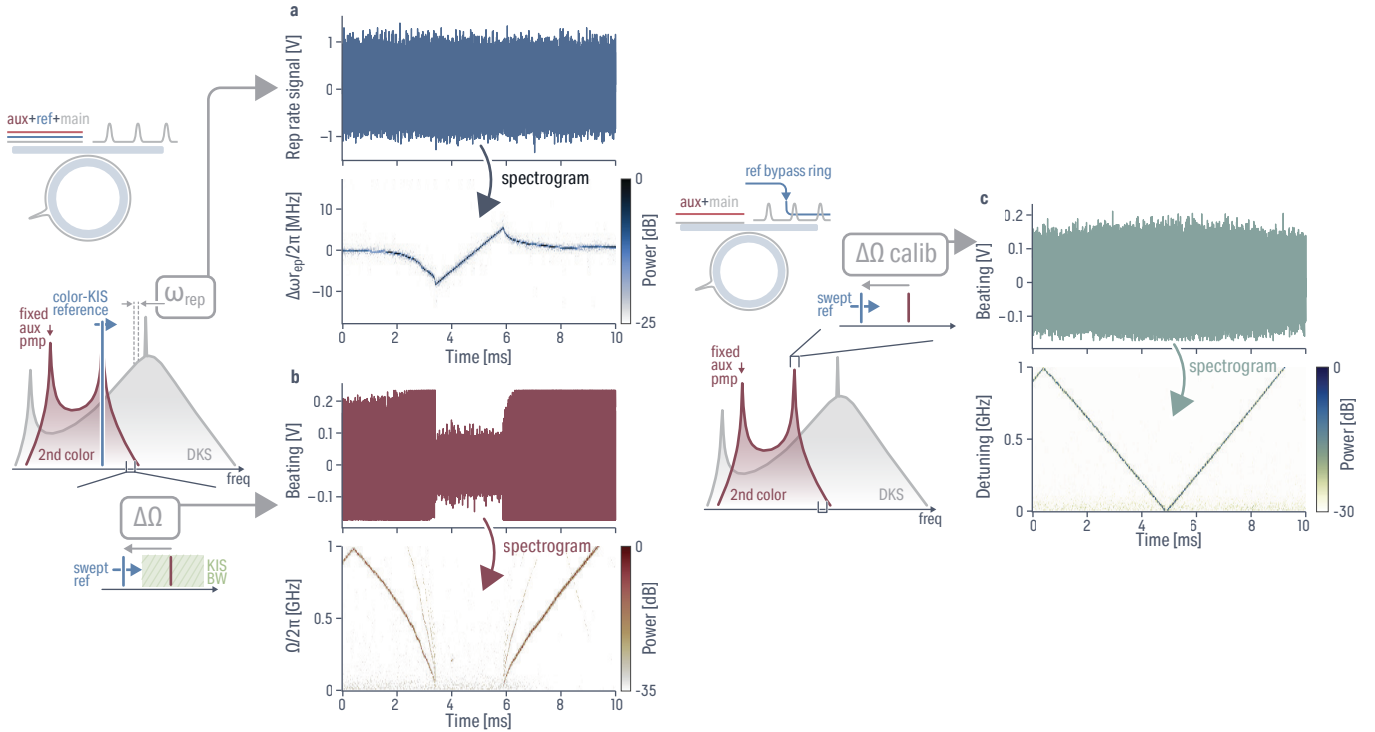
Fig. S.2 – Repetition rate, detuning beat note and calibration protocols. **a-b** Simultaneous measurement of the repetition rate ω_{rep} and the beat note between the reference and the second color Ω. We record the temporal trace while sweeping the reference laser with a triangular waveform that actuates the CTL piezo element. The direction of the sweep is known from the CTL characteristics: high-to-low voltage results in high-to-low reference laser frequency, and the oscilloscope is triggered on the raising slope of the triangular waveform. Applying a consecutive fast Fourier transform (through the *scipy* python package [5]) allows us to retrieve the instantaneous frequency of the signal. **c** Calibration of the detuning to convert the temporal frequency trace from the spectrogram maxima in **a** and **b**, performed for each $\Delta\mu$ presented in **??**. We bypass the resonator with the reference laser and beat it directly against the second color comb tooth. We record the temporal trace and apply a fast Fourier transform to retrieve the instantaneous frequency. In this calibration nonlinear effects associated with the reference laser cannot occur, and the detuning against the comb tooth can be directly obtained, including the zero reference for the detuning. The obtained frequency beat is flipped if needed according to knowledge if the detuning is positive or negative based on the triangular waveform applied.

a spectrogram with a clear peak for each time sample that correspond to either $\delta\omega_{\text{beat}}$, from which we extract ω_{rep} using the RF synthesizer frequency and the number of comb teeth as previously described, or Ω.

However, the detuning needs to be calibrated accurately. We harness the fact that the frequency comb, if unsynchronized, can act as a local oscillator. To this extent, for each of the different $\Delta\mu$ measurements shown in **??**, we proceed to calibrate the detuning by bypassing the microresonator with the reference and directly beating it with the closest secondary color comb tooth (*i.e.*, no nonlinearity present since we bypass the ring, and hence no KIS) as shown in Fig. S.2c. Once again, we proceed to obtain the spectrogram from the temporal trace, from which we can calibrate the detuning over time, with a precise calibration of the zero-detuning (*i.e.* position of the secondary color comb tooth). We note that we obtain the absolute value of the detuning and need to process to change its sign based on the direction of the triangular waveform applied to the CTL piezo element. From knowledge of the CTL characteristics, we know that a high-to-low voltage results in a high-to-low frequency, hence the detuning is negative for times before the calibration frequency reaches zero, since the oscilloscope is triggered for positive slope with the piezo ramp signal.

S.3. Laser phase noise measurement

We lock the 1300 nm and 1500 nm CTLs using independent 10 MHz free spectral range (FSR) Mach-Zenhder interferometers (MZIs), and using a Pound-Drever-Hall technique allows us to actuate the current and piezo element of the laser (respectively fast and slow feedback) to lock to the side of a fringe of the MZI [Fig. S.3]. To measure their respective phase noise, we use another MZI with a 40 MHz FSR. Setting the laser to be at a quadrature point of this MZI, we measure the residual MZI noise using a real time electrical spectum analyzer (RSA). Understanding the noise obtained from the MZI [Fig. S.3b], we can retrieve the frequency noise of the laser following:
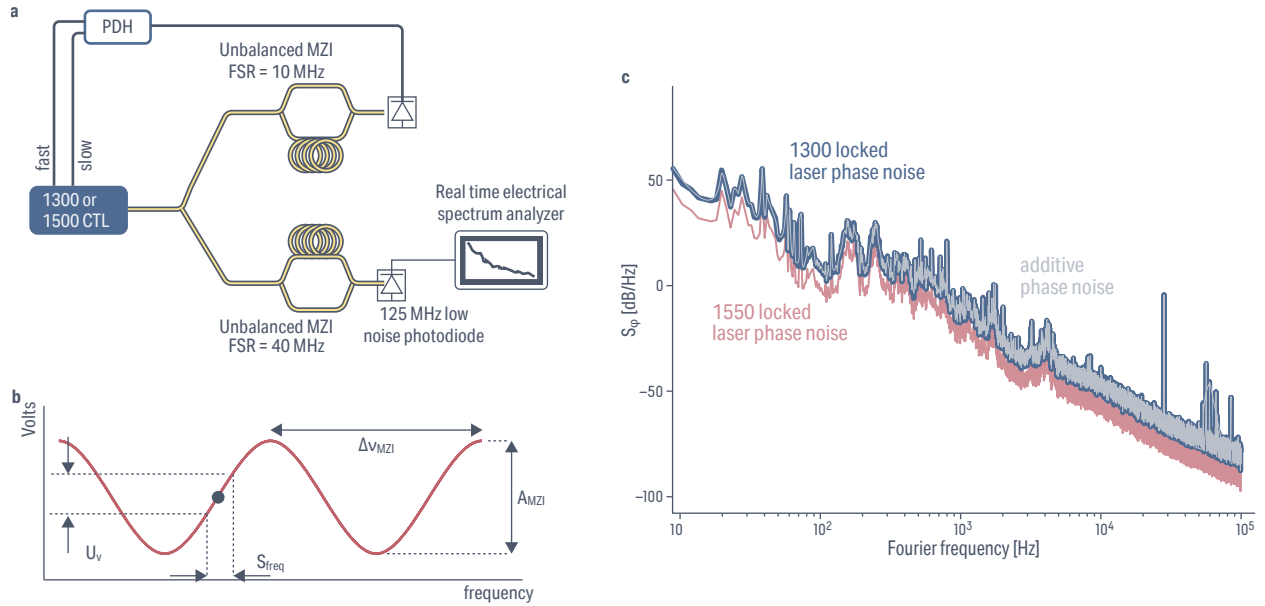
Fig. S.3 – **Phase noise characterization of the auxiliary and reference pump. a** Schematic of the experimental setup to measure the auxiliary or reference laser phase noise. We lock the laser to an unbalanced fiber Mach-Zehnder interferometer (MZI) with a 10 MHz free spectral range. We measure the phase noise of the laser using another 40 MHz MZI, and a low noise 125 MHz photodiode. **b** Schematic explaining the relationship between the noise measured with the 40 MHz FSR MZI and the laser frequency noise. **c** Phase noise of the 1300 nm laser (blue) and 1550 nm laser (red). The phase noise of the 1300 nm laser is larger than the 1550 nm laser, and if accounting for additive noise between them (gray) shows that it is predominantly noise from the 1300 nm laser. The power is referenced to that of the carrier, namely, dBc/Hz

$$ S_\nu = \left[\frac{\Delta\nu_{\mathrm{MZI}}}{\pi} \sin^{-1}\left(\frac{U_{\mathrm{MZI}}}{A_{\mathrm{mzi}}} \right) \right]^2 \quad [\mathrm{Hz}^2/\mathrm{Hz}] $$

with $U_{\mathrm{MZI}} = \sqrt{50 \times 10^{-3} \times 10^{S_{\mathrm{MZI}}/10}}$ the voltage obtained from spectral measurement, where S_{MZI} is the optical power in decibels normalized to 1 mW of the MZI noise at quadrature (i.e., in dBm), the spectrum analyzer impedance is assumed to be 50 Ω, $A_{\mathrm{mzi}} = 584$ mV is the amplitude of the sinusoidal modulation with frequency of the MZI, and $\Delta\nu_{\mathrm{MZI}} = 40$ MHz is the free spectral range of the MZI used for noise measurement.

We can obtain the phase noise from the frequency noise, where the power is referenced to that of the carrier, namely, dBc/Hz:

$$ S_\varphi = 10 \log_{10}\left(\frac{S_\nu}{\nu^2} \right) \quad [\mathrm{dB/Hz}] $$

When comparing the phase noise of the two locked lasers, the 1500 nm laser exhibits lower noise Fig. S.3. When accounting for additive noise since the two lasers are locked to independent MZIs, as the 1300 nm laser being more noisy than the 1500 nm laser, the noise of the 1300 nm laser is predominant. We therefore consider OFD of the 1300 nm laser noise when assessing the repetition rate noise under color-KIS.

S.4. Leveraging the cooler as an auxiliary pump for counter-propagating color-KIS

In order to demonstrate that color-KIS can occur with a limited set of lasers, we leverage the fact that we already use a cooler pump to thermally stabilize the microring resonator for adiabatic access to the soliton. While in the main text of the manuscript we use a cross-polarized cooler pump (transverse magnetic polarization) relative to the main pump (transverse electric polarization) to minimize the nonlinearity induced by the cooler, here we instead operate in the same polarization to allow the cooler to also act as an auxiliary pump that creates a second soliton color and new set of DWs. Since the cooler is high power, even synthetic DWs on the opposite side of the pump than the reference (i.e., a different sign for μ) and which are usually inefficient can be created [Fig. S.4a], enabling a larger OFD factor than
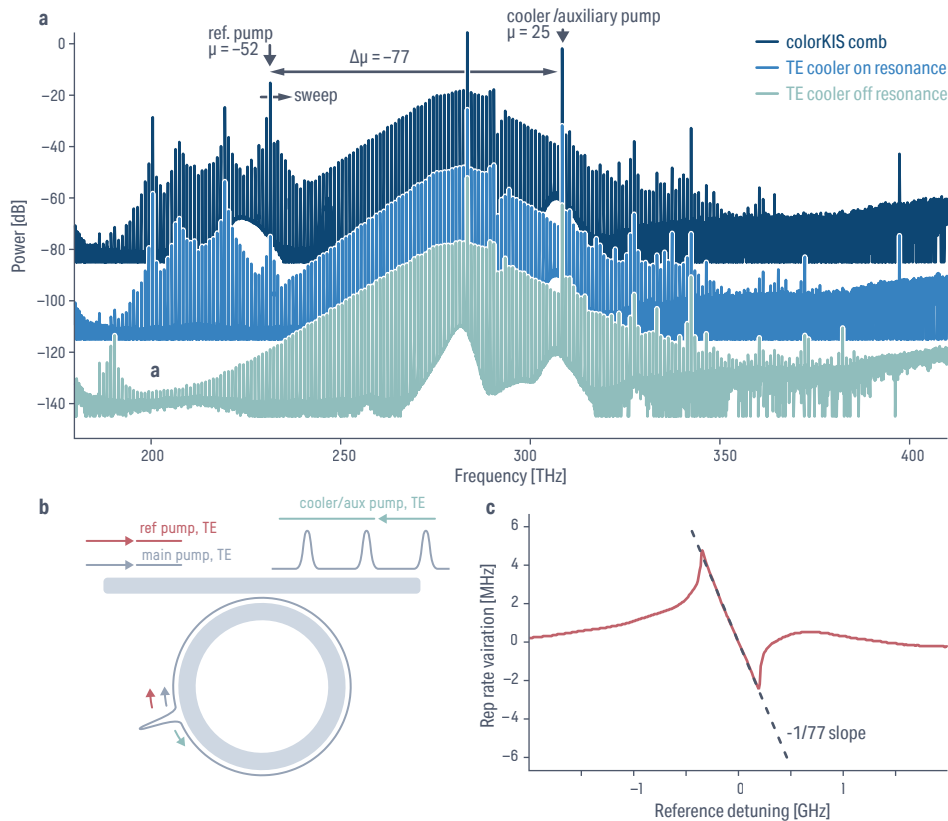
Fig. S.4 – **Counter-propagating cooler pump used as the auxiliary pump for synthetic DW creation and counter-propagating color-KIS. a** Optical frequency comb with the transverse electric counter-propagating cooler set off resonance such that its induced nonlinearity is minimized (foreground spectrum in teal). When the cooler is set to be on resonance, it acts as an auxiliary pump that creates a new set of colors with the synthetic DWs at $\mu = -52$ and $\mu = -82$, while through cascading a third color is also created with other synthetic DWs (middle spectrum in light blue). Hence, we can use the reference laser at the synthetic DW created by the cooler/auxiliary pump laser, enabling color-KIS with a limited number of lasers (background spectrum in dark blue). **b** Schematic of the counter-propagating color-KIS scheme. Here, the cooler laser also acts as an auxiliary pump that mediates the creation of a new soliton color and synthetic dispersive waves. Instead of using the cooler in the same propagation direction as the reference and main pumps, we can leverage that since KIS is XPM-mediated, it can even be triggered in a counter-propagating fashion. **c** The repetition rate entrainment follows the slope defined by the cooler and auxiliary pump mode spacing, which, since the cooler is of such high power, enables a larger OFD than presented in the main text. Here, the auxiliary/cooler pump and reference pump are on opposite sides of the main pump, whereas in the main text they were set with a μ of the same sign.

presented in the main text. Interestingly, this effect still occurs despite the cooler remaining in a counter-propagating direction relative to the main and reference pump [Fig. S.4b]. As KIS is mediated through cross-phase modulation, counter-propagating KIS can happen, as previously demonstrated between two counter-propagating solitons [6], where the synchronization is mediated by coherent backscattering, which we believe is also the case in our work. However, in linear transmission measurements we do not observe lifting of the resonance degeneracy between the two traveling wave modes at either the reference mode or at the cooler mode, and hence the synchronization could be mediated by a relatively weak backscattering relative to the resonance linewidth, or by Rayleigh scattering at other modes where the secondary color exists. Regardless, we leverage the resulting synthetic dispersive wave for large OFD, while also simplifying the architectural complexity of color-KIS by reducing the number of required lasers. We send a reference at $\mu = -52$ while the cooler is present at $\mu = +25$, enabling an OFD of $\Delta\mu = -77$, which is confirmed by repetition rate entrainment measured at the DKS comb component [Fig. S.4c].

[1] S. Zhang, J. M. Silver, L. Del Bino, F. Copie, M. T. M. Woodley, G. N. Ghalanos, A. Ø. Svela, N. Moroney, and P. Del'Haye, Sub-milliwatt-level microresonator solitons with extended access range using an auxiliary laser, Optica **6**, 206 (2019).
[2] H. Zhou, Y. Geng, W. Cui, S.-W. Huang, Q. Zhou, K. Qiu, and C. Wei Wong, Soliton bursts and deterministic dissipative Kerr soliton generation in auxiliary-assisted microcavities, Light: Science & Applications **8**, 50 (2019).

[3] J. R. Stone and S. B. Papp, Harnessing Dispersion in Soliton Microcombs to Mitigate Thermal Noise, Physical Review Letters **125**, 153901 (2020).

[4] G. Moille, J. Stone, M. Chojnacky, R. Shrestha, U. A. Javid, C. Menyuk, and K. Srinivasan, Kerr-induced synchronization of a cavity soliton to an optical reference, Nature **624**, 267 (2023).

[5] P. Virtanen, R. Gommers, T. E. Oliphant, M. Haberland, T. Reddy, D. Cournapeau, E. Burovski, P. Peterson, W. Weckesser, J. Bright, S. J. van der Walt, M. Brett, J. Wilson, K. J. Millman, N. Mayorov, A. R. J. Nelson, E. Jones, R. Kern, E. Larson, C. J. Carey, İ. Polat, Y. Feng, E. W. Moore, J. VanderPlas, D. Laxalde, J. Perktold, R. Cimrman, I. Henriksen, E. A. Quintero, C. R. Harris, A. M. Archibald, A. H. Ribeiro, F. Pedregosa, and P. van Mulbregt, SciPy 1.0: Fundamental algorithms for scientific computing in Python, Nature Methods **17**, 261 (2020).

[6] Q.-F. Yang, X. Yi, K. Y. Yang, and K. Vahala, Counter-propagating solitons in microresonators, Nature Photonics **11**, 560 (2017)